

Application Study of Newton-Raphson-Type Nonlinear MPC for Hydrostatic Transmissions Under Disturbance and System Uncertainty

Dang Ngoc Danh
 Chair of Mechatronics
 University of Rostock
 Rostock D-18059, Germany
 Ngoc.Dang@uni-rostock.de

Harald Aschemann
 Chair of Mechatronics
 University of Rostock
 Rostock D-18059, Germany
 Harald.Aschemann@uni-rostock.de

Abstract—Model predictive control (MPC) is well established and has a huge practical relevance in many industrial applications, especially for chemical or thermal plants. This paper presents the design and the implementation of a nonlinear model predictive control aiming at an accurate tracking control of desired output trajectories under disturbances and uncertainties for a nonlinear hydrostatic transmission system with multiple control inputs, which represents a fast mechatronic system. The benefit of this solution is that it can be easily adapted to either velocity tracking control or torque tracking control – which is not the case with alternative model-based approaches. The control design is based on a numerical optimization within a moving horizon using the Newton-Raphson method in combination with the optimization-over-some-variables technique. The unmeasurable system state variables as well as the system disturbances are reconstructed by an unscented Kalman filter which is well suited for nonlinear systems subject to process and measurement noise. The proposed control scheme is investigated by simulations and experimentally validated on a test rig at the Chair of Mechatronics, University of Rostock. The results indicate the robustness of the proposed control structure by a high tracking accuracy despite system disturbances and uncertainties.

Index Terms—Multivariable Systems, Hydrostatic Transmission, Model Predictive Control, Real-Time Implementation

I. INTRODUCTION

Hydrostatic transmissions (HSTs) offer many advantages over other forms of power transmissions such as high power density, a continuously varying and large transmission ratio, low inertia, reversion of the motion direction without changing gears, dynamic braking and flexible geometrical arrangements, cf. [1], [2]. They are widely used in industrial applications like heavy working machines for construction and agriculture as well as off-road vehicles, cf. [3]. They are recently employed also in wind turbines and power-split gearboxes, cf. [4]. HSTs typically consist of a hydraulic pump and a hydraulic motor connected in a closed circuit by means of hydraulic hoses. The pump is coupled to the prime mover and the motor is coupled to the load. The mechanical power supplied to the

Dang Ngoc Danh is also associated with the Faculty of Engineering, Vietnam National University of Agriculture, Hanoi, Vietnam, Dndanh@vnua.edu.vn

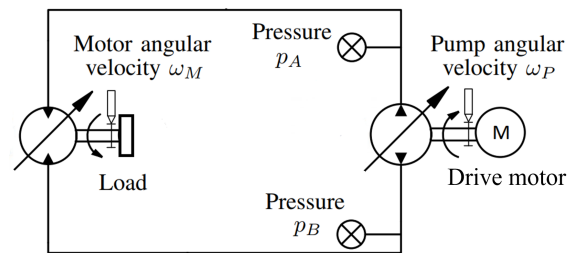


Fig. 1. Principle structure of an HST system.

system is transformed into hydraulic power and transmitted to the hydraulic motor in the form of a pressurized fluid flow. Here, it is transformed back into mechanical power, see Fig. 1. There are several designs of the hydraulic pump and motor. Among them, the axial piston type with a variable volumetric displacement is the most popular and provides most versatile control means for applications, cf. [1]. Thanks to this structure, the transmission ratio is adjustable by altering the swash-plate angle of the hydraulic pump, by altering the axial bent angle of the hydraulic motor or by a simultaneously variation of both. As a result, both torque and angular velocity of the hydraulic motor can be controlled independently according to the purpose of the specific application.

For the tracking control of hydrostatic transmission systems, several concepts have already been proposed. Many of them deal with the system as a single-input single-output (SISO) system as in [5]–[7], in which only the pump displacement is used for actuation purposes. More advanced control approaches for multiple-input multiple-output (MIMO) systems have been developed afterwards. In [8] and [9], a nonlinear model-based control approach has been proposed and validated for the tracking control of the angular velocity. For this control, a second desired output - the difference pressure - is required and derived from the desired value of the angular velocity. The result shows a good tracking performance when dealing with both control inputs for hydraulic pump and motor simultaneously. In [16], a decentralized approach has been proposed

which allows for a significant improvement of the tracking control performance. In this design, the MIMO system is decomposed into two SISO subsystems, where the motor bent-axis angle and the control of pump swash-plate angle are treated separately. For the tracking control, the desired trajectory of angular velocity and the desired bent-axis angle are required, and they are supposed to be synchronized with respect to each other to guarantee the envisaged transmission ratio.

This contribution extends the conference paper presented in [17] with more technical details and a new application study. A nonlinear model predictive control is investigated for the tracking of either the angular velocity or the hydraulic torque by adjusting the control inputs of both displacement units appropriately: the motor bent-axis angle and the pump swash-plate angle. This corresponds to the framework of multiple-input single-output (MISO) system, which allows for a relaxation of the design of a second output trajectory as in [16] and avoids a singularity at zero when tracking the pressure difference as pointed out in [8]. The tracking performance is assessed by both simulations and experiments. The corresponding test rig, for which a validated model is available, has been built up at the Chair of Mechatronics, University of Rostock, see Fig. 2.



Fig. 2. HST test rig at the Chair of Mechatronics, University of Rostock.

II. SYSTEM MODELLING

The details for the following mathematical model derivation of the HST can be found in [16]. Therefore, the system modelling is presented only briefly.

A. Hydraulic Subsystem

Pump Flow Rate: The pump flow rate

$$q_P = \frac{V_P(\alpha_P)\omega_P}{2\pi} \quad (1)$$

is proportional to the angular velocity ω_P of the pump. The nonlinear dependence of the volumetric displacement $V_P(\alpha_P)$ on the tilt angle of the swash plate α_P is given by

$$V_P(\alpha_P) = N_P A_P D_P \tan(\alpha_{P,\max} \cdot \tilde{\alpha}_P), \quad (2)$$

with the normalized swash-plate angle $\tilde{\alpha}_P = \alpha_P/\alpha_{P,\max}$. The effective piston area A_P , the diameter D_P of the piston circle, and the number N_P of pistons represent geometric parameters. With $\tilde{V}_P = \frac{N_P A_P D_P}{2\pi}$ denoting the maximum volumetric displacement, the pump flow rate becomes

$$q_P = \tilde{V}_P \tan(\alpha_{P,\max} \cdot \tilde{\alpha}_P) \omega_P. \quad (3)$$

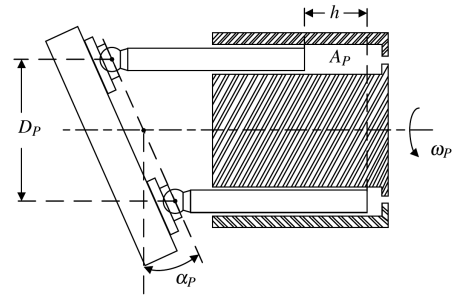


Fig. 3. Swash-plate mechanism of the hydraulic pump.

Motor Flow Rate: The hydraulic motor is characterized by a bent-axis design. The volume flow rate

$$q_M = \frac{V_M(\alpha_M)\omega_M}{2\pi} \quad (4)$$

is proportional to the motor angular velocity ω_M . The volumetric displacement of the motor $V_M(\alpha_M)$ is subject to a nonlinear dependence on α_M . Given the geometrical parameters N_M , A_M , and D_M , the volume flow rate can be expressed as

$$q_M = \tilde{V}_M \sin(\alpha_{M,\max} \cdot \tilde{\alpha}_M) \omega_M. \quad (5)$$

Here, $\tilde{\alpha}_M = \alpha_M/\alpha_{M,\max}$ denotes the normalized bent-axis angle and $\tilde{V}_M = \frac{N_M A_M D_M}{2\pi}$ the maximum volumetric displacement of the hydraulic motor.

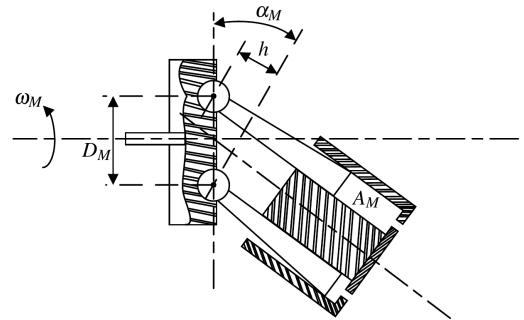


Fig. 4. Bent-axis mechanism of the hydraulic motor.

Dynamics of the difference pressure: To keep the model order small, the difference pressure between the high and low pressure sides is introduced as state variable. Assuming symmetric physical conditions and negligible pressure losses in the hydraulic hoses, the difference pressure is governed by the following differential equation

$$\Delta \dot{p} = \frac{2}{C_H} \left(\tilde{V}_P \tan(\alpha_{P,\max} \cdot \tilde{\alpha}_P) \omega_P - \tilde{V}_M \sin(\alpha_{M,\max} \cdot \tilde{\alpha}_M) \omega_M \right) - \frac{q_U}{C_H}, \quad (6)$$

where the lumped disturbance q_U accounts for leakage flows, and C_H stands for the hydraulic capacitance.

Dynamics of Actuators: For both the pump and the motor, the dynamics of the displacement units is characterized by a first-order lag behaviour according to

$$\begin{aligned} T_{u_P} \dot{\tilde{\alpha}}_P + \tilde{\alpha}_P &= k_P u_P, \\ T_{u_M} \dot{\tilde{\alpha}}_M + \tilde{\alpha}_M &= k_M u_M. \end{aligned} \quad (7)$$

Here, T_{u_P} and T_{u_M} denote the corresponding time constants, and k_P and k_M the proportional gains. Moreover, u_P and u_M are the inputs of the servo valves. According to the physical design, both the control inputs and the angles are bounded: $u_P \in [-1, 1]$, $u_M \in [\epsilon_M, 1]$, $\tilde{\alpha}_P \in [-1, 1]$ and $\tilde{\alpha}_M \in [\epsilon_M, 1]$, $\epsilon_M > 0$.

B. Mechanical Subsystem

The equation of motion of the HST system is given by the first-order dynamics

$$J_V \dot{\omega}_M + d_V \omega_M = \tilde{V}_M \Delta p \sin(\alpha_{M,\max} \cdot \tilde{\alpha}_M) - \tau_U. \quad (8)$$

Here d_V is the damping coefficient, and J_V the mass moment of inertia. The lumped disturbance torque τ_U takes into account load disturbances as well as model uncertainty.

C. The Nonlinear Model of the Overall System

The dynamics of the HST system is obtained by combining the subsystem descriptions derived above. The nonlinear fourth-order state space description becomes

$$\begin{bmatrix} \dot{\tilde{\alpha}}_M \\ \dot{\tilde{\alpha}}_P \\ \Delta \dot{p} \\ \dot{\omega}_M \end{bmatrix} = \begin{bmatrix} -\frac{1}{T_{u_M}} \tilde{\alpha}_M + \frac{k_M}{T_{u_M}} u_M \\ -\frac{1}{T_{u_P}} \tilde{\alpha}_P + \frac{k_P}{T_{u_P}} u_P \\ \frac{2\tilde{V}_P}{C_H} \tan(\alpha_P) \omega_P - \frac{2\tilde{V}_M}{C_H} \sin(\alpha_M) \omega_M - \frac{q_U}{C_H} \\ -\frac{d_V}{J_V} \omega_M + \frac{\tilde{V}_M}{J_V} \sin(\alpha_M) \Delta p - \frac{\tau_U}{J_V} \end{bmatrix}, \quad (9)$$

where $\alpha_M = \tilde{\alpha}_M \cdot \alpha_{M,\max}$ as well as $\alpha_P = \tilde{\alpha}_P \cdot \alpha_{P,\max}$ are employed. The two control inputs are given by u_P and u_M .

III. NONLINEAR MODEL PREDICTIVE CONTROL DESIGN

The design of the nonlinear model predictive control (NMPC) is based on the nonlinear system model in discrete-time form, where the future states are predicted within a finite moving prediction horizon based on the current states and corresponding input values. The minimization of the cost function over the prediction horizon results in a suboptimal input sequence, where only the first control action is applied to the system. Then, this procedure is repeated for the next time step.

A. Definition of the Cost Function

The cost function for the NMPC design is usually chosen in a standard way as a quadratic function of both the system states and the control inputs. In this application study, however, it turns out that the specification of a suitable cost function, which is not in standard form, is crucial for attaining of the desired tracking performance of the MISO system. The specification of the cost function is derived from an analysis of the HST system in operation. As illustrated in Fig. 5, the operation of a hydrostatic transmission – using both variable volumetric

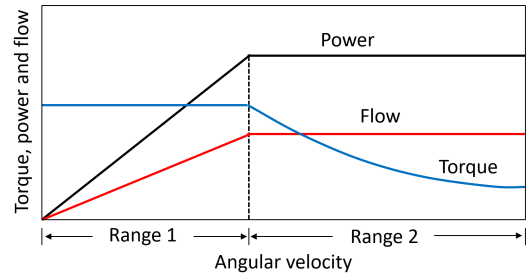


Fig. 5. Performance characteristics of the HST.

displacements of the pump and the motor simultaneously – can be divided into two principle operating ranges. In range 1, the motor displacement is fixed to the maximum value, whereas the pump displacement increases from zero to the maximum value. The torque remains constant as the pump displacement increases, but both power and volume flow are proportional to the angular velocity. Range 2 begins when the pump reaches its maximum displacement, and now the motor displacement is reduced with increasing angular velocity. Within this range, the torque is inversely proportional to the angular velocity, while the power remains constant, cf. [1]. In practical applications, it is usually required to attain the highest torque possible at the motor shaft, which is equivalent to keeping the motor displacement as large as possible. This characteristic is, hence, reflected in the definition of the cost function J for the prediction horizon comprising N points, with time steps k , according to

$$J = \sum_{k=1}^N [w_1 (r - \omega_{M,k})^2 + w_2 \Delta p_k^2 + w_3 (1 - \tilde{\alpha}_{M,k})^2 + w_4 (p - \tilde{\alpha}_{P,k})^2]. \quad (10)$$

Here, positive scalars w_1, w_2, w_3, w_4 represent the weights for the individual cost terms, and $p \in [0, 1]$ denotes a fixed design parameter. They all serve as hyperparameters in the predictive control design. The first term in the cost function penalizes the error between the output ω_M and its reference value r , the second term has a smoothing effect on the movements of the displacement units to avoid oscillations in the system. The deviation of the motor bent-axis angle $\tilde{\alpha}_M$ from its maximum is penalized by the third term, whereas the final term, regarding the pump swash-plate angle $\tilde{\alpha}_P$, is a practical measure to smoothen transitions from one displacement unit to the other.

B. Numerical Optimization Method

The computational burden regarding the online optimization is still one of the most predominant issues in a real-time implementation of NMPC, especially for fast mechatronic applications. In the case of the hydrostatic transmission system, the system model consists of four states and two input variables, which renders the selection of optimization technique crucial for the real-time implementation of the NMPC on the available hardware configuration. Aiming at a small computational effort in real-time, the dynamic optimization is turned into a static optimization problem by a numerically

direct evaluation of the cost function with the system dynamics and using the well-known Newton-Raphson algorithm with its favourable convergence properties. Here, given box constraints for the feasible ranges of the inputs and states are also taken into account within the numerical optimization process.

The implementation involves the discretization of the system model using numerical methods such as explicit Euler, Euler-Heun or Runge-Kutta integration. Here, the computational burden which is related to the discretization methods also needs to be taken into account to guarantee both real-time capability and an efficient implementation on the available hardware. Simulation tests have been conducted, and the performance of each discretization technique is presented in Table I. From the statistics in Table I it becomes obvious that,

TABLE I
PERFORMANCE OF DISCRETIZATION METHODS

Performance	Discretization Method		
	Euler	Euler-Heun	Runge-Kutta
RMS error	4.279e-1	2.571e-1	2.219e-1

in comparison with the explicit Euler method, the Euler-Heun approach reduces the RMS error by 40%, whereas the Runge-Kutta method achieves an error reduction by 48%. Given the larger computational effort that is related to the higher number of evaluations of the right hand side of the state equations, the Euler-Heun method is, obviously, a better choice regarding calculation effort and performance.

Deploying the Euler-Heun method, the system model is time-discretized in the form of a predictor-corrector scheme. By defining the state vector $\mathbf{x} = [\tilde{\alpha}_M \ \tilde{\alpha}_P \ \Delta p \ \omega_M]^T$ and the control input vector $\mathbf{u} = [u_M \ u_P]^T$, the continuous-time nonlinear dynamics function according to (9)

$$\mathbf{f}(\mathbf{x}, \mathbf{u}) = \begin{bmatrix} -\frac{1}{T_{uM}}\tilde{\alpha}_M + \frac{k_M}{T_{uM}}u_M \\ -\frac{1}{T_{uP}}\tilde{\alpha}_P + \frac{k_P}{T_{uP}}u_P \\ \frac{2\tilde{V}_P}{C_H}\tan(\alpha_P)\omega_P - \frac{2\tilde{V}_M}{C_H}\sin(\alpha_M)\omega_M - \frac{q_U}{C_H} \\ -\frac{d_V}{J_V}\omega_M + \frac{\tilde{V}_M}{J_V}\sin(\alpha_M)\Delta p - \frac{\tau_U}{J_V} \end{bmatrix} \quad (11)$$

is replaced by a discrete-time one. The discrete evaluation of the system variables at each time step k is denoted by \mathbf{x}_k and $\mathbf{f}(\mathbf{x}_k, \mathbf{u}_k)$, and the prediction model becomes

$$\mathbf{x}_{k+1} = \mathbf{x}_k + T_s \frac{\mathbf{f}(\mathbf{x}_k, \mathbf{u}_k) + \mathbf{f}(\bar{\mathbf{x}}_k, \mathbf{u}_k)}{2}, \quad (12)$$

where

$$\bar{\mathbf{x}}_k = \mathbf{x}_k + T_s \mathbf{f}(\mathbf{x}_k, \mathbf{u}_k), \quad (13)$$

represents an Euler step and T_s is the sampling time. The cost function J according to (10) accumulates while the future system behaviour is predicted in the finite horizon.

The application of the Newton-Raphson algorithm is based on the numerical evaluation of both the gradient and the Hessian of the cost function J w.r.t. the optimization variables. In this scheme, the optimization variables are given by the

control input sequences $u_{M,k}$ and $u_{P,k}$. They are stacked in a vector \mathbf{u}_{opt} as follows

$$\mathbf{u}_{opt} = [u_1, \dots, u_N, u_{N+1}, \dots, u_{2N}], \quad (14)$$

where first N control inputs from u_1, \dots, u_N correspond to the control input u_M and the remaining N ones u_{N+1}, \dots, u_{2N} are related to the control input u_P . The computation of the full Hessian matrix would be quite expensive regarding the dimension of the optimization problem. With N points of time contained in the prediction horizon, the number of optimization variables becomes $2N$, hence, resulting in a Hessian matrix of the dimension $2N \times 2N$. Note that each element in the control sequence may take an arbitrary value in the feasible input space independent of the others. Considering the convexity of the local optimization problem, the calculation of the full gradient and the full Hessian matrix can be avoided, and this reduces the computational load significantly. By applying the optimizing-over-some-variables technique, see [15] for details, the gradient and the Hessian matrix are reduced to scalars, i.e., the first and the second derivatives of the cost function J w.r.t. a selected element in \mathbf{u}_{opt} . This allows for a large number of Newton steps within the given sampling time interval - even in the case of the fast mechatronic system with a sampling time of 50 msec. Please note that similar ideas are also used in stochastic gradient descent. Here, however, the sequence of optimization variables is predefined. Fig. 6 illustrates the search process in a constrained search space using the mentioned technique for the simple example of a convex optimization problem with only two independent variables. As can be seen, during the iteration one variable is updated after the other until the search terminates close to the minimum.

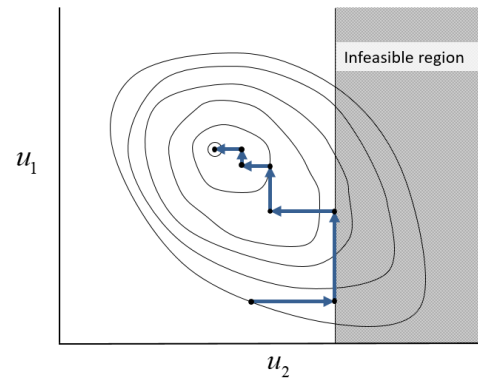


Fig. 6. Illustration of the optimization process following the idea of optimizing-over-some-variables in the case of two optimization variables.

The numerical evaluation of the first and second derivatives of the cost function J w.r.t. the j -th element of \mathbf{u}_{opt} can be performed using the central difference formula, cf. [10], as follows

$$\begin{aligned} \frac{\partial J}{\partial u_j} &= \frac{J_{u_j+\Delta u} - J_{u_j-\Delta u}}{2\Delta u}, \\ \frac{\partial^2 J}{\partial u_j^2} &= \frac{J_{u_j+\Delta u} - 2J_{u_j} + J_{u_j-\Delta u}}{\Delta u^2}. \end{aligned} \quad (15)$$

Here, Δu is a small positive number defining the perturbation of the control element u_j , and J_{u_j} denotes the corresponding value of the cost function when the control element u_j is applied to the system. Other notations regarding J are interpreted in similar manner. The update rule, which takes into account the inputs constraints, is given by:

$$u_j^*(i+1) = u_j(i) - \frac{\partial J}{\partial u_j} \left(\frac{\partial^2 J}{\partial u_j^2} \right)^{-1},$$

$$u_j(i+1) = \begin{cases} a, & \text{if } u_j^*(i+1) < a \\ u_j^*(i+1), & \text{if } a \leq u_j^*(i+1) \leq b \\ b, & \text{if } u_j^*(i+1) > b \end{cases} \quad (16)$$

Here, the index i defines the i -th iteration of the optimization algorithm, and a and b are the lower and upper bounds of the input variables, respectively.

The state constraints, which are identical to the constraints of the control inputs in the given case, are applied only to two variables – the normalized pump swash-plate angle $\tilde{\alpha}_P$ and normalized the motor bent-axis angle $\tilde{\alpha}_M$. It is worth noting that these two state variables are governed by first-order lag systems with proportional gains k_P and k_M , which are both equal to 1. This implies that the state constraints are automatically satisfied as long as the control inputs remain in their bounded regions.

C. Summary of the Optimization Algorithm

Initialize $\mathbf{u}_{opt} = \mathbf{0}$
 Read current state vector \mathbf{x}_k and disturbances from the UKF
 For $i = 1$ to maximal number of iterations i_{max}
 For $j = 1$ to $2N$
 • Calculate the derivatives:
 ◊ Initialize the cost function $J = 0$
 ◊ Disturb the control element $u_{opt,j}$ with Δu
 ◊ Predict the state \mathbf{x}_{k+1} in the horizon using (12)
 ◊ Accumulate the cost function according to (10)
 ◊ Calculate gradient and Hessian with (15)
 • Update the control input $u_j(i+1)$ according to (16)
 End
 End
 Apply $[u_M, u_P]^T = [u_{opt,1}, u_{opt,N+1}]^T$ to the real system.

D. Stability Analysis

The stability of the proposed NMPC algorithm needs still to be addressed. Many systematic approaches have been proposed to guarantee the stability of NMPC algorithms, however, their success is limited to specific cases due to a lack of conservativeness in general, cf. [12]. In this study, the cost function is not given in the standard formulation, which is even harder for a stability proof in a systematic way. The stability analysis, instead, aims at finding evidence for the stability of the designed control structure and the error convergence. For this purpose, the cost function is considered at time step k within the prediction horizon, which is defined by

$$V_k = w_1(r - \omega_{M,k})^2 + w_2(\Delta \dot{p}_k)^2 + w_3(1 - \tilde{\alpha}_{M,k})^2 + w_4(p - \tilde{\alpha}_{P,k})^2. \quad (17)$$

Since this function is positive definite and radially unbounded, it can be used as a Lyapunov function candidate. Applying the theorem of non-monotonic Lyapunov functions for the stability of discrete-time nonlinear system, see [13] for details, results in the following stability condition

$$(V_{k+N} - V_k) + \dots + (V_{k+1} - V_k) < 0. \quad (18)$$

This criterion is numerically evaluated over the prediction horizon using the optimal control sequence \mathbf{u}_{opt} . As the criterion is satisfied, Fig. 11 shows strictly negative values, (18) implies a decreasing Lyapunov function candidate over the control horizon, which indicates the stability of the control system.

IV. SYSTEM VARIABLES ESTIMATION

The implementation of the proposed NMPC requires the feedback of all system states and, moreover, the estimation of unknown disturbances. Taking into account the high nonlinearity of the system model as well as the effects of disturbances and measurement noise, an extended Kalman filter would be suitable for the reconstruction of these system variables. In this study, however, an unscented Kalman filter (UKF), see [11], is preferred because it promises superior estimation results. For this purpose, the state vector in system (9) is extended by corresponding disturbance models for the load torque and the leakage volume flow. This leads to

$$\mathbf{x}_e = [\tilde{\alpha}_M \quad \tilde{\alpha}_P \quad \Delta p \quad \omega_M \quad q_U \quad \tau_U]^T, \quad (19)$$

where two integrators are introduced as disturbance models according to

$$\begin{bmatrix} \dot{q}_U \\ \dot{\tau}_U \end{bmatrix} = \begin{bmatrix} 0 \\ 0 \end{bmatrix}. \quad (20)$$

The measured outputs are given by

$$\mathbf{y}_m = \begin{bmatrix} \Delta p \\ \omega_M \end{bmatrix} = \begin{bmatrix} 0 & 0 & 1 & 0 & 0 & 0 \\ 0 & 0 & 0 & 1 & 0 & 0 \end{bmatrix} \mathbf{x}_e = \mathbf{C}_m \mathbf{x}_e. \quad (21)$$

The system is again discretized by means of the Euler-Heun method, which results in a similar representation as in (12)

$$\mathbf{x}_{e,k+1} = \mathbf{x}_{e,k} + T_s \frac{\Phi(\mathbf{x}_{e,k}, \mathbf{u}_k) + \Phi(\bar{\mathbf{x}}_{e,k}, \mathbf{u}_k)}{2}, \quad (22)$$

with the Euler prediction step

$$\bar{\mathbf{x}}_{e,k} = \mathbf{x}_{e,k} + T_s \Phi(\mathbf{x}_{e,k}, \mathbf{u}_k). \quad (23)$$

Here, Φ is a nonlinear function presenting the dynamics of the extended system

$$\Phi = \begin{bmatrix} -\frac{1}{T_{uM}} \tilde{\alpha}_{M,k} + \frac{k_M}{T_{uM}} u_{M,k} \\ -\frac{1}{T_{uP}} \tilde{\alpha}_{P,k} + \frac{k_P}{T_{uP}} u_{P,k} \\ \frac{2\tilde{V}_P}{C_H} \tan(\alpha_{P,k}) \omega_{P,k} - \frac{2\tilde{V}_M}{C_H} \sin(\alpha_{M,k}) \omega_{M,k} - \frac{q_{U,k}}{C_H} \\ -\frac{d_V}{J_V} \omega_{M,k} + \frac{\tilde{V}_M}{J_V} \sin(\alpha_{M,k}) \Delta p_k - \frac{\tau_{U,k}}{J_V} \\ 0 \\ 0 \end{bmatrix} \quad (24)$$

Both the state equations and the measurement equation are extended by mean-free Gaussian white noise processes. The

details of UKF design follows the ideas presented in [14] as well as [18] and involves the choice of a set of $2n + 1$ sigma points

$$\chi_{i,k} = \begin{cases} \mathbf{x}_{e,k}, & i = 0 \\ \mathbf{x}_{e,k} + \eta(\sqrt{\mathbf{P}_{x,k}})_i, & i = 1, \dots, n \\ \mathbf{x}_{e,k} - \eta(\sqrt{\mathbf{P}_{x,k}})_i, & i = n + 1, \dots, 2n, \end{cases} \quad (25)$$

where $(\sqrt{\mathbf{P}_{x,k}})_i$ represents the i -th column of the matrix square root of $\mathbf{P}_{x,k}$, which can be determined by a Cholesky decomposition, see [14]. The dimension of the extended state vector is given by n , and η represents a scaling factor defined as

$$\eta = \alpha^2 (n + \kappa). \quad (26)$$

The constants α and κ characterize the spread of the sigma points, which is important for the sampling of the propability density. The associated weights of the states and covariances are determined according to

$$w_{m,i} = \begin{cases} \frac{\lambda}{\lambda+n}, & i = 0 \\ \frac{1}{2(\lambda+n)}, & i = 1, \dots, 2n \end{cases} \quad (27)$$

$$w_{c,i} = \begin{cases} \frac{\lambda}{\lambda+n} + (1 - \alpha^2 + \beta), & i = 0 \\ w_{m,i}, & i = 1, \dots, 2n, \end{cases}$$

where $\lambda = \eta - n$ holds. Furthermore, β is a scalar related to the higher-order distribution of the sigma points. As a Gaussian distribution is assumed, with covariance matrices w.r.t. process noise \mathbf{Q} and measurement noise \mathbf{R} , the choice $\beta = 2$ is optimal. Given this setting, the UKF algorithm repeats the following steps at each sampling time:

- Nonlinear transformation of the sigma points and calculation of the mean value

$$\chi_{k+1} = \chi_k + T_s \Phi(\mathbf{x}_{e,k}, \mathbf{u}_k)$$

$$\tilde{\mathbf{x}}_{e,k+1} = \sum_{i=0}^{2n} w_{m,i} \chi_{i,k+1}$$

- Prediction of the error covariance matrix

$$\tilde{\mathbf{P}}_{x,k+1} = \sum_{i=0}^{2n} w_{c,i} (\chi_{i,k+1} - \tilde{\mathbf{x}}_{e,k+1}) (\chi_{i,k+1} - \tilde{\mathbf{x}}_{e,k+1})^T + \mathbf{Q}$$

- Prediction of the measurements

$$\gamma_{k+1} = \mathbf{C}_m \chi_{k+1}$$

$$\tilde{\mathbf{y}}_{k+1} = \sum_{i=0}^{2n} w_{m,i} \gamma_{i,k+1}$$

- Prediction of the measurement error covariance matrix

$$\mathbf{P}_{y,k+1} = \sum_{i=0}^{2n} w_{c,i} (\gamma_{i,k+1} - \tilde{\mathbf{y}}_{k+1}) (\gamma_{i,k+1} - \tilde{\mathbf{y}}_{k+1})^T + \mathbf{R}$$

- Calculation of the cross-covariance matrix and update of the Kalman gain \mathbf{K}

$$\mathbf{P}_{xy,k+1} = \sum_{i=0}^{2n} w_{c,i} (\chi_{i,k+1} - \tilde{\mathbf{x}}_{e,k+1}) (\gamma_{i,k+1} - \tilde{\mathbf{y}}_{k+1})^T$$

$$\mathbf{K}_{k+1} = \mathbf{P}_{xy,k+1} \mathbf{P}_{y,k+1}^{-1}$$

- Updates of the state vector and the error covariance matrix

$$\mathbf{x}_{e,k+1} = \tilde{\mathbf{x}}_{e,k+1} + \mathbf{K}_{k+1} (\mathbf{y}_k - \tilde{\mathbf{y}}_{k+1})$$

$$\mathbf{P}_{x,k+1} = \tilde{\mathbf{P}}_{x,k+1} - \mathbf{K}_{k+1} \mathbf{P}_{y,k+1} \mathbf{K}_{k+1}^T$$

The implementation of the estimator-based NMPC is illustrated in Fig. 7.

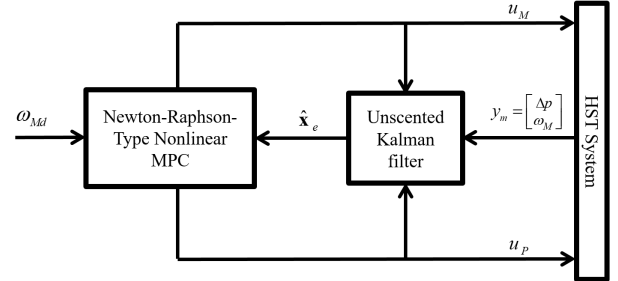


Fig. 7. Implementation of the overall estimator-based NMPC structure.

V. INVESTIGATION OF THE CONTROL STRUCTURE

A. Simulation Results

The simulations are performed using a step size of $T_s = 50$ msec. Aiming at realistic and reliable simulation results, the output signals are extended by additive measurement noise, and the disturbance torque and leakage volume flow are modelled as follows

$$q_U = 1 \cdot 10^{-12} \Delta p,$$

$$\tau_U = 0.1 J_V \dot{\omega}_M + 7 \tanh\left(\frac{\omega_M}{0.1}\right). \quad (28)$$

The prediction horizon is selected as $N = 5$ by trial-and-error but in compliance with the stability analysis. In the sequel, two alternative control objectives are investigated:

- Tracking of the desired angular velocity $\omega_{Md}(t)$
- Tracking of the desired hydraulic torque $\tau_{Md}(t)$ of the motor.

Please not that the flexibility in choosing the controlled variable is a benefit of this predictive control approach. In other model-based control schemes, larger modifications would be necessary to attain a similar flexibility. Each of control objectives is studied in two application scenarios:

- In the first scenario, the angular velocity of the hydraulic pump and the load torque applied to the motor shaft are constant.
- In the second scenario, both the the angular velocity and load torque are harmonically varying.

1) *Tracking Control of the Angular Velocity:* In the first scenario, the hydraulic pump speed is set to 700 rpm and the load torque is held constant at 0 Nm. Moreover, the weights of cost function are selected as $w_1 = 8e4$, $w_2 = 1e-6$, $w_3 = 10e5$, $w_4 = 11e4$ and $p = 0.6$. Results w.r.t. the trajectory tracking of the desired motor angular velocity ω_{Md} are shown in Fig. 8 and Fig. 9. As can be seen, a very high tracking

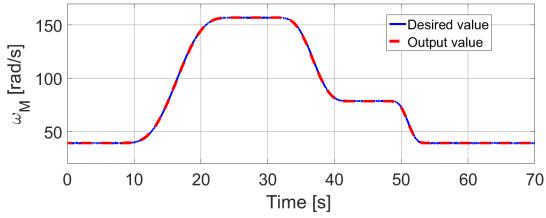


Fig. 8. Comparison of simulated values and desired values for the motor angular velocity ω_M .

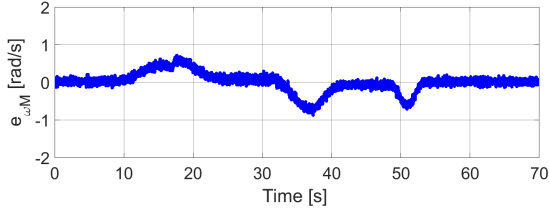


Fig. 9. Tracking errors w.r.t. the motor angular velocity (simulation results).

performance is achieved with only small errors between the controlled output and the desired values.

The variations of both displacement units, see Fig. 10, meet the constraints and show the envisaged characteristic. When the pump swash-plate angle is still within its admissible working range, the motor maintains its maximal volume displacement. If the pump displacement unit reaches the saturation value, the motor displacement decreases to enlarge the motor angular velocity for an accurate tracking. The

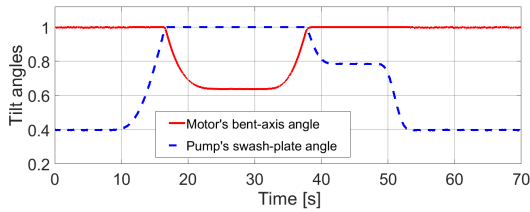


Fig. 10. Synchronous variations of the displacement units (simulation results).

stability criterion (18) is evaluated during the tracking process. The numerical results with strictly negative values indicate a constant decrease of the Lyapunov function candidate over the prediction horizon during the complete tracking process as can be seen in Fig. 11.

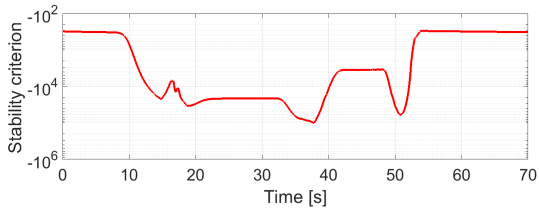


Fig. 11. Evaluation of NMPC stability criterion, which gives strictly negative values during the tracking process (simulation results, depicted on a logarithmic scale).

For the second test scenario, both the hydraulic pump angular velocity and external load torque are assumed to vary periodically as shown in Figs. 12 and 13. This mimics the working conditions in real applications where the drive engine changes the angular velocity due to external effects or due to the operator. In addition, the load may also vary due to external resistances. Such conditions happen frequently in applications of hydrostatic transmission in wind turbines or in working machines.

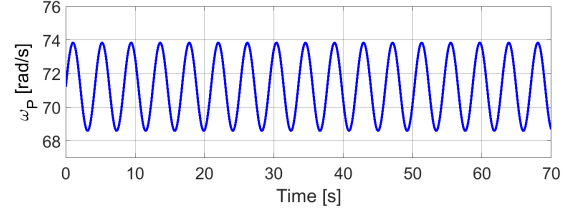


Fig. 12. Variation of the hydraulic pump angular velocity.

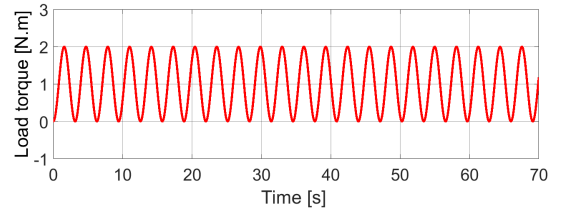


Fig. 13. Variation of the external load torque.

Fig. 14 shows the tracking result w.r.t. the angular velocity under the harmonic variation of both pump angular velocity and load torque acting on the hydraulic motor shaft. A good tracking performance is still achievable, however, a small periodic oscillation is visible in the controlled output.

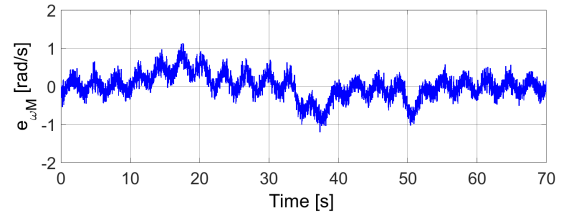


Fig. 14. Velocity tracking error subject to an external disturbance (simulation results).

2) *Tracking Control of the Hydraulic Torque:* For the objective of hydraulic torque tracking, the first term in the cost function, which penalizes the tracking error, is modified accordingly. The altered cost function reads

$$J_{\tau} = \sum_{k=1}^N \left[w_{\tau 1} (r_{\tau} - \tau_{M,k})^2 + w_{\tau 2} \Delta \dot{p}_k^2 + w_{\tau 3} (1 - \tilde{\alpha}_{M,k})^2 + w_{\tau 4} (p_{\tau} - \tilde{\alpha}_{P,k})^2 \right], \quad (29)$$

where the hydraulic torque $\tau_{M,k}$ is evaluated according to

$$\tau_{M,k} = \tilde{V}_M \sin(\alpha_{M,k}) \Delta p_k \quad (30)$$

and r_τ is the corresponding desired torque value. The corresponding weights are selected as $w_{\tau 1} = 4.5e7$, $w_{\tau 2} = 5.1e-7$, $w_{\tau 3} = 1.5e7$, $w_{\tau 4} = 9e6$ and $p_\tau = 0.6$. Figs. 15 and 16 depicts simulation results for the hydraulic torque tracking without disturbance impact, i.e. with a constant pump speed and a vanishing external load torque. Fig. 17 shows the

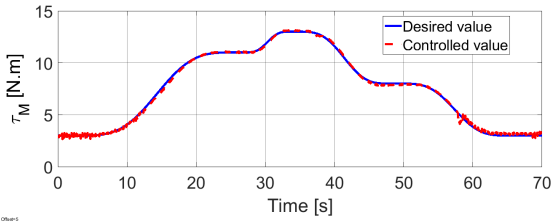


Fig. 15. Comparison of desired and simulated values for the hydraulic torque.

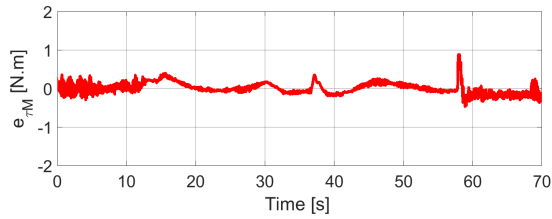


Fig. 16. Simulated tracking errors of the hydraulic torque without external disturbances.

tracking result of hydraulic torque tracking under harmonic variations of both the pump angular velocity and the external load torque. As can be seen, the controller is still able to maintain an accurate tracking, however, superposed by a small remaining oscillation caused by the disturbances.

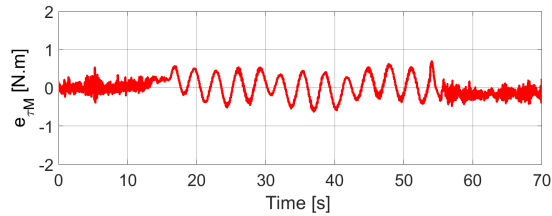


Fig. 17. Simulated tracking errors of the hydraulic torque subject to harmonic external disturbances.

B. Experiments on the Test Rig

1) *Angular Velocity Tracking Control:* The control structure is implemented on a dedicated test rig using an identical sampling time of $T_s = 50$ msec. The parameters implemented on the test rig are based on simulations but slightly altered for a better performance: $w_1 = 2.3e4$, $w_2 = 4e-6$, $w_3 = 3.1e5$, $w_4 = 2.5e4$ and $p = 0.6$.

Experimental results for the tracking error w.r.t. the angular velocity are shown in Fig. 19. A little non-smooth change of the error is visible at the transition between the two displacement units. The accuracy, however, is still comparable

to the one seen in the simulation study. This indicates a high quality of the simulation model. Fig. 20 depicts the behaviour of the motor bent-axis angle and the pump swash-plate angle in experiments on the real system, which are also similar to the simulation results.

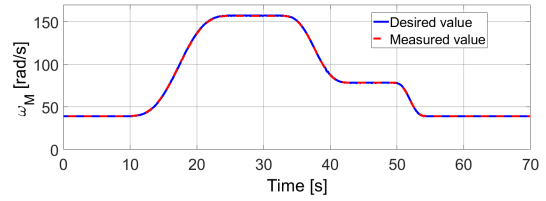


Fig. 18. Tracking of the motor angular velocity at the test rig.

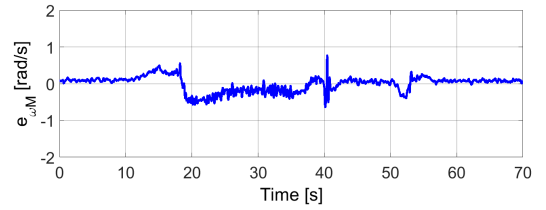


Fig. 19. Tracking errors for the motor angular velocity at the test rig.

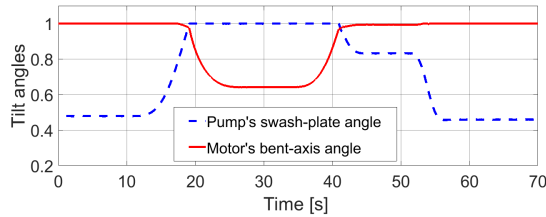


Fig. 20. Variations of the displacement units at the test rig.

For the test case subject to disturbance effects, the tracking result for the motor angular velocity is shown in Fig. 21. A slightly increase of the tracking error can be recognized accompanied by oscillations, similar to the simulation results. Nevertheless, a high tracking accuracy is still achievable which indicates the capabilities of the proposed control design.

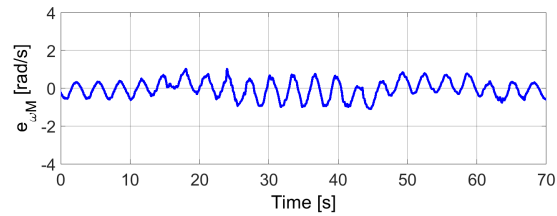


Fig. 21. Angular velocity tracking error of the real system under an external disturbance

2) *Hydraulic Torque Tracking Control:* For the experiments regarding a tracking of the hydraulic motor torque, the weights are implemented as follows: $w_{\tau 1} = 9.3e6$, $w_{\tau 2} = 5.1e-7$,

$w_{\tau 3} = 5.3e7$, $w_{\tau 4} = 2e6$ and $p_{\tau} = 0.6$. The error w.r.t. to the tracking of the hydraulic torque on the test rig is depicted in Fig. 23. As can be seen, a highly accurate tracking becomes possible with a maximum error of only 3% of the input range.

Under the impact of disturbances, a good tracking behaviour

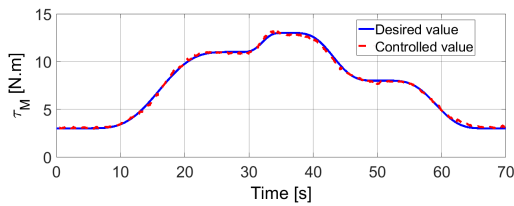


Fig. 22. Tracking of hydraulic torque at the test rig without additional external disturbances.

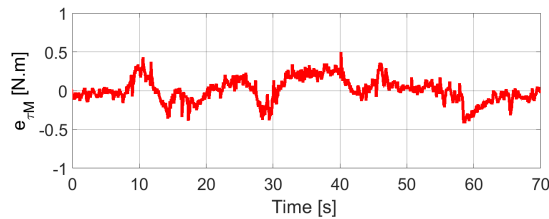


Fig. 23. Tracking error of the hydraulic torque at the test rig without additional external disturbances.

for the hydraulic torque is still maintained as shown in Fig. 24. Similar to the case of angular velocity tracking, however, the error plot also reveals a slight remaining oscillation caused by the disturbance.

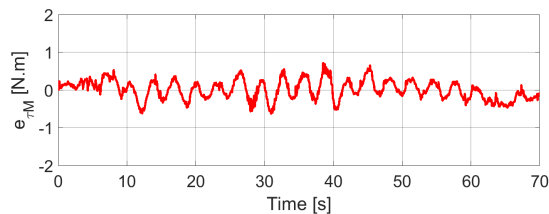


Fig. 24. Hydraulic torque tracking error at the test rig with additional external disturbances.

VI. CONCLUSIONS

In this paper, a nonlinear model predictive control has been implemented on a hydrostatic transmission test rig for the tracking control of either the desired angular velocity or the desired hydraulic torque – which offers a high flexibility for the user. The real-time implementation is based on a numerical optimization by means of a Newton-Raphson-type algorithm. To enable the use for this fast mechatronic system, the algorithm is simplified and tailored to achieve a small computational effort but, at the same time, to deal with two constrained input variables for an accurate control of the highly nonlinear system. The NMPC takes advantage of state estimates as well as disturbance estimates provided

by an unscented Kalman filter. Simulations and experimental results from a test rig indicate a high accuracy and a good performance of the nonlinear control structure that counteracts efficiently both model uncertainty and external disturbances.

REFERENCES

- [1] A. Hitchcox, Engineering essentials: Hydrostatic transmissions. Hydraulics & Pneumatics, 2016.
- [2] H. Aschemann and H. Sun, “Decentralised flatness-based control of a hydrostatic drive train subject to actuator uncertainty and disturbances,” In Proc. of Conf. on Methods and Models in Automation and Robotics (MMAR), pp. 759–764, 2013.
- [3] H. Schulte, “Control-oriented modeling of hydrostatic transmission using Takagi-Sugeno fuzzy systems,” In Proc. of IEEE Intern. Fuzzy Systems Conference, pp. 1–6, 2007.
- [4] H. Schulte, “Control-oriented description of large scale wind turbines with hydrostatic transmission using Takagi-Sugeno models. In Proc. of Conf. on Control Applications (CCA), pp. 664–668, 2014.
- [5] J. Kwaśniewski, J. Pluta and A. Piotrowska, “Research on the properties of a hydrostatic transmission with different controllers,” In Acta Montanistica Slovaca, vol. 8, pp. 240–244, 2003.
- [6] H. W. Wu and C. B. Lee, “Self-tuning adaptive speed control for hydrostatic transmission systems,” In Intern. Journal of Computer Applications in Technology, vol. 9, pp. 18–33, 1996.
- [7] J. Lennevi and J. O. Palmberg, “Application and implementation of LQ design method for the velocity control of hydrostatic transmissions,” In Proc. of Institution of Mechanical Engineers, vol. 209, pp. 255–268, 1995.
- [8] H. Aschemann J. Ritzke and H. Schulte, “Model-based nonlinear trajectory control of a drive chain with hydrostatic transmission,” In Proc. of Conf. on Methods and Models in Automation and Robotics (MMAR), 2009.
- [9] J. Ritzke and H. Aschemann, “Design and experimental validation of nonlinear trajectory control of a drive chain with hydrostatic transmission,” In Proc. of Scandinavian Int. Conf. on Fluid Power (SICFP), 2011.
- [10] R. K. Arora, Optimization: Algorithms and Applications. Taylor & Francis Group, New York, USA, 2015.
- [11] E. Wan and R. Van der Merwe, “The unscented Kalman filter for nonlinear estimation,” In Proc. of IEEE Conf. on Adaptive Systems for Signal Processing, Communications, and Control Symposium, pp. 153–158, 2000.
- [12] W. H. Chen, “Stability analysis of classic finite horizon model predictive control,” In International Journal of Control, Automation, and Systems, vol. 8(2), Springer, pp. 187–197, 2010.
- [13] A. A. Ahmadi and P. A. Parrilo, “Non-monotonic Lyapunov functions for stability of discrete time nonlinear and switched systems,” In Proc. of IEEE Conf. on Decision and Control, 2008.
- [14] S. J. Julier and J. K. Uhlmann, “Unscented filtering and nonlinear estimation,” In Proc. of the IEEE, vol. 92(3), pp. 401–422, 2004.
- [15] S. Boyd and L. Vandenberghe, Convex Optimization. Cambridge University Press, 2009.
- [16] H. Sun, Decentralized nonlinear control for a hydrostatic drive train with unknown disturbances. PhD thesis, University of Rostock, Shaker, 2015.
- [17] N. D. Dang and H. Aschemann, “Real-time implementation of model predictive multivariable tracking control for hydrostatic transmissions,” In Proc. of Intern. Conf. on System Theory, Control and Computing (ICSTCC), pp. 343–348, 2020.
- [18] N. D. Dang and H. Aschemann, “Discrete-time state-dependent proportional-integral control for torque tracking of hydrostatic transmissions,” IFAC PapersOnLine, vol 53(2), pp. 6591–6596, 2020.